Preprints of the 19th World Congress
The International Federation of Automatic Control
Cape Town, South Africa. August 24-29, 2014

Compressive Sampling in Intensity Based Control for Adaptive Optics

Elisabeth Brunner, * **João Silva,** * **Cornelis de Visser,** **
Michel Verhaegen *

* *Delft Center for Systems and Control, Faculty of Mechanical, Maritime, and Materials Engineering, Delft University of Technology, Delft 2628 CD, The Netherlands. (E-mail: A.E.Brunner@tudelft.nl).*
** *Control and Simulation Division, Faculty of Aerospace Engineering, Delft University of Technology, Delft 2600 CD, The Netherlands.*

Abstract: The central problem in Adaptive Optics feedback control is the reconstruction of the aberrated wavefront from wavefront sensor measurements. We recently presented a novel algorithm to compute the wavefront estimate directly from (Shack-)Hartmann intensity images instead of using the classical centroid algorithm to approximate the local wavefront slopes. The novel algorithm allows a distributed linearization of the model describing the imaging process through the use of a B-spline parametrization of the wavefront. This linearization enables the estimation of the wavefront via a linear least-squares solver. A major bottleneck of this new algorithm is the computational complexity that stems from the large number of pixels with each pixel giving rise to one row of the overdetermined set of equations. In this paper, a compression method is proposed to speed up this new reconstruction method by only using a small percentage of the given intensities to make it applicable for real-time Adaptive Optics. Numerical simulations for open- and closed-loop show that reducing the data on the one hand dramatically reduces the number of measurements, but on the other hand does not cause any significant loss in accuracy or robustness of the reconstructed wavefront estimate.

Keywords: Image restoration, Output feedback control, Linearization, Data compression

1. INTRODUCTION

The main limitations to high resolution imaging in fields as microscopy, lithography or ground based astronomy are caused by aberrations in the phase profile, the so called wavefront, of light waves. In observations with ground based telescopes the aberrations are mainly introduced by the turbulent atmosphere of the Earth. Adaptive Optics (AO)[Hardy, 1998] is used to compensate for the wavefront distortions in real-time. A sensor measures information from which the aberration is reconstructed and then corrected with a deformable mirror (DM). The wavefront reconstruction (WFR) is the crucial part of a classical real-time AO system, since the bandwith of the feedback controller is much smaller than the first resonance frequency of the deformable mirror. With the increasing dimensionality of the new generation of extremely large telescopes, there is urgent demand for computationally efficient reconstruction methods.

For this reason, the most common class of wavefront sensors is the (Shack-)Hartmann sensor which allows the formulation of the reconstruction problem as a linear (least-squares) problem. This paper is restricted to a Hartmann sensor, but the results are extendable to the Shack-Hartmann architecture. A Hartmann sensor consists of an array of apertures which sample the incoming wavefront by approximating the local spatial slopes of the wavefront using the center of mass of the intensity measurements collected by a detector. Since not all the information present in the intensity patterns is used, this approach results in loss of accuracy of the wavefront estimate.

Silva et al. [2013] recently proposed a novel method based on a distributed linearization of the relationship between the local wavefront aberrations in each subaperture and the corresponding intensity pattern in the detector. This approach preserves the linearity of the reconstruction problem, and it makes direct use of the intensity measurements as done by Polo et al. [2012] instead of using the center of gravity of the pixel pattern computed with the centroid algorithm [Carvalho, 2004]. The unknown wavefront is parametrized and reconstructed with B-splines, a methodology presented in our recent work by De Visser and Verhaegen [2013].

The major advantage of this new method is the increased accuracy with which the wavefront can be estimated, by not using the approximation of the wavefront slopes but the intensity measurements provided by the Hartmann sensor. However, this results in higher computational complexity of the wavefront reconstruction which has to be applied in real-time. The contribution of this paper is a methodology to reduce the number of used intensity measurements which results directly in a linear speed up of the computational cost. Inspired by the technique of compressive sampling [Candès, 2006], we can show that a small percentage of the measurements is sufficient to

⋆ This work was supported in part by the Dutch NOVA partnership in the European Strategy Forum on Research Infrastructures (ESFRI).

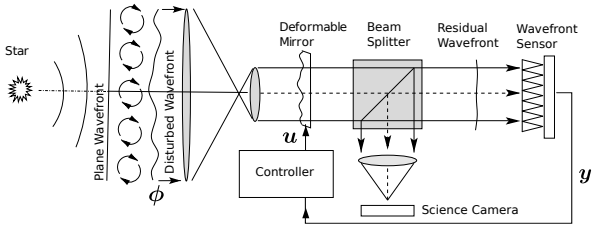

Fig. 1. Scheme of a closed-loop AO system.

reconstruct the wavefront with nearly the same accuracy. The paper is organized as follows. After a brief introduction of the novel spline based method for intensity measurements in Section 3, a procedure selecting the intensity measurements which are most sensitive to our linear model is presented with a short analysis of the achieved computational gain in Section 4. A simulation study in Section 5 analyzes the performance of the new method using only 10% of the intensity measurements. Next to a comparison with the classical modal reconstruction method for slope measurements [Southwell, 1980], it is shown that the compressive sampling approach preserves accuracy and robustness of the original method for intensity measurements for open- and closed-loop configuration. We consider a classical AO feedback control described in a control engineering framework e.g. in [Hinnen et al., 2007, 2008]. Further, a perfect mirror and static wavefront aberrations are assumed. Finally, we end this paper with some concluding remarks.

2. THE ADAPTIVE OPTICS CONTROL PROBLEM

To explain the role of wavefront reconstruction in the closed-loop of an AO system, we briefly outline the principle of astronomical AO on the basis of the schematic drawing in Figure 1. The light emitted from a distant point source, arrives as a plane wave at the outer layers of the Earth's atmosphere. Crossing the turbulent atmosphere, time and space varying optical path differences are introduced, such that the wave reaches the telescope with a distorted phase profile $\phi(\boldsymbol{x}, t)$, where $\boldsymbol{x} \in \mathbb{R}^2$ denotes the spatial position in the telescope aperture and t the time. The AO system aims at correcting those wavefront aberrations by introducing optical path differences of opposite sign through an active component, the deformable mirror. Light entering the AO system is first directed to the deformable mirror, whose shape is adjusted in real-time to apply a time-varying phase correction $\phi_{\mathrm{DM}}(\boldsymbol{x}, t)$. After the wavefront correction, a beam splitter sends one part of the light to a science camera. The remaining light is directed to a wavefront sensor (WFS) which measures the uncorrected residual phase error $\phi_{\mathrm{res}}(\boldsymbol{x}, t) = \phi(\boldsymbol{x}, t) - \phi_{\mathrm{DM}}(\boldsymbol{x}, t)$. Based on the wavefront measurements $\boldsymbol{y}$, a feedback controller has to compute the actuator inputs $\boldsymbol{u}$ to the DM. The common approach is to first reconstruct an estimate $\phi^*(\boldsymbol{x}, t)$ of the wavefront from the wavefront measurements, and to then compute actuator commands $\boldsymbol{u}$ such that the applied phase $\phi_{\mathrm{DM}}(\boldsymbol{x}, t)$ cancels out most of the estimated aberrations. In this paper, we assume a perfect mirror which implies that the DM can perfectly compensate the estimated wavefront, i.e. phase $\phi_{\mathrm{DM}}(\boldsymbol{x}, t) = \phi^*(\boldsymbol{x}, t)$. In the following section, the wavefront reconstruction problem is solved for a Hartmann wavefront sensor.

3. SPLINE BASED WAVEFRONT RECONSTRUCTION FROM INTENSITY MEASUREMENTS

A Hartmann wavefront sensor consists of an array of apertures wich are equally spaced in an otherwise opaque screen. The wavefront is sampled by each subaperture in the aperture plane and the transmitted beams are collected by e.g. a CCD camera in the detector plane [Polo et al., 2012]. In this section, we briefly introduce the main principles of the novel method introduced by Silva et al. [2013]. After the derivation and local linearization of the model which describes the relationship between the wavefront and the intensity measurements, the parametrization of the unknown wavefront with B-splines and the computation of the estimate as a constrained least-squares (LS) solution are described.

3.1 Linearized phase retrieval problem

The complex field $U(x, y, z)$ of a wave transmitted by the Hartmann hole array can be computed as function of the wave's amplitude $A(x, y)$ and phase distribution $\phi(x, y)$. In the aperture plane $z = 0$ and the detector plane $z = L$, $U(x, y, z)$ is respectively given by

$$U(x, y, 0) = A(x, y) \exp(ik\Phi(x, y)) \,, \tag{1}$$

$$U(x, y, L) = \mathscr{F}^{-1} \left[\mathscr{F}[U(x, y, 0)] H(f_x, f_y) \right] \,, \tag{2}$$

with $H(f_x, f_y)$ denoting the Rayleigh-Sommerfield transfer function [Goodman, 2005] for spatial frequencies f_x and f_y. For a wavelength λ, the wavenumber is defined as $k = \frac{2\pi}{\lambda}$.

We parametrize the wavefront $\phi(x, y)$ in (1) as a linear combination

$$\phi(x, y) = \sum_{k=1}^{K} \alpha_k f_k(x, y) \tag{3}$$

of K basis functions $f_k(x, y)$. Given is a set of intensity measurements $I_{\mathrm{meas}}(x_i, y_j)$ from the Hartmann sensor's CCD camera and a model of the measurements triggered by an imcoming wavefront $\phi(x, y)$ is provided with (2) as $I(x_i, y_j, L) = |U(x_i, y_j, L)|^2$[Goodman, 2005]. An estimate of weighting coefficients α_k can then be computed by minimizing the error between the measured and modeled intensities which yields the cost function

$$J = \sum_{i,j} \left[I_{\mathrm{meas}}(x_i, y_j) - I(x_i, y_j, L) \right]^2 = ||\boldsymbol{i}_{\mathrm{meas}} - \boldsymbol{i}_L||_2^2 \,, \tag{4}$$

where the intensity vectors are defined as $\boldsymbol{i}_{\mathrm{meas}}(m) = I_{\mathrm{meas}}(m)$ and $\boldsymbol{i}_L(m) = I(m, L)$ with each index $m = 1, ..., M$ corresponding to a pixel center location (x_i, y_j) in the detector.

A truncated first order Taylor expansion for a constant coefficient vector $\bar{\boldsymbol{\alpha}} \in \mathbb{R}^{K \times 1}$ approximates the nonlinear imaging model by

$$I(m, L) \approx I(m, L)\big|_{\bar{\boldsymbol{\alpha}}} + \frac{\partial I(m, L)}{\partial \boldsymbol{\alpha}}\Big|_{\bar{\boldsymbol{\alpha}}} \boldsymbol{\alpha} := c_{0m} + (\boldsymbol{c}_{\mathbf{1}m})^{\mathrm{T}} \boldsymbol{\alpha} \,. \tag{5}$$

Applying this linearization for each pixel $m = 1, ..., M$, one obtains a constant vector $\boldsymbol{c_0} := [c_{01}, ..., c_{0M}]^{\mathrm{T}} \in \mathbb{R}^{M \times 1}$ and the constant Jacobian matrix $\mathbf{C_1} := [\boldsymbol{c}_{\mathbf{1}1}, ..., \boldsymbol{c}_{\mathbf{1}M}]^{\mathrm{T}} \in \mathbb{R}^{M \times K}$. The cost function of the linearized wavefront reconstruction problem can then be defined as

$$J_{\mathrm{lin}} = ||\boldsymbol{i}_{\mathrm{meas}} - (\boldsymbol{c_0} + \mathbf{C_1}\boldsymbol{\alpha})||_2^2 \,. \tag{6}$$

With the optimal least-squares solution

$$\boldsymbol{\alpha}^* := ((\mathbf{C_1})^{\mathrm{T}}\mathbf{C_1})^{-1}(\mathbf{C_1})^{\mathrm{T}}(\boldsymbol{c_0} - \boldsymbol{i}_{\mathrm{meas}})\,, \tag{7}$$

the reconstructed wavefront can be computed with the basis expansion in (3).

3.2 Multivariate simplex B-splines

De Visser and Verhaegen [2013] suggested to use multivariate B-splines [De Visser, 2011] to expand the wavefront in (3). This type of basis functions can be used as an alternative for this expansion as well as the linearization outlined in Section 3.1. For the sake of brevity, we continue to use the same notation as in (5) to represent the linearization as obtained in terms of the B-spline coefficients.

B-splines are defined locally on simplices, which correspond in the 2 dimensional case to triangles t, each defined by 3 non-degenerate vertices $(\boldsymbol{v_0}, \boldsymbol{v_1}, \boldsymbol{v_2}) \in \mathbb{R}^{2\times 3}$, and evaluated for $\boldsymbol{x} = (x, y) \in \mathbb{R}^2$ with the Barycentric coordinate system. For a simplex t with vertices $(\boldsymbol{v_0}, \boldsymbol{v_1}, \boldsymbol{v_2})$, the Barycentric coordinates (b_0, b_1, b_2) of a point $\boldsymbol{x}$ in the Cartesian plane are given by

$$\begin{bmatrix} b_1 \\ b_2 \end{bmatrix} = \mathbf{V}^{-1} \begin{bmatrix} x \\ y \end{bmatrix}\,, \quad b_0 = 1 - b_1 - b_2\,, \tag{8}$$

with transformation matrix $\mathbf{V} = [\boldsymbol{v_1} - \boldsymbol{v_0}, \boldsymbol{v_2} - \boldsymbol{v_0}]$. On the simplex t, the Bernstein polynomials

$$B^d_\kappa(b(\boldsymbol{x})) = \begin{cases} \dfrac{d!}{\kappa_0!\kappa_1!\kappa_2!} b_0^{\kappa_0} b_1^{\kappa_1} b_2^{\kappa_2} & , \boldsymbol{x} \in t \\ 0 & , \boldsymbol{x} \notin t \end{cases} \tag{9}$$

of degree d, with $|\kappa| = \kappa_0 + \kappa_1 + \kappa_2 = d$ and $\kappa_0, \kappa_1, \kappa_2 \geq 0$ give a local basis. A linear combination of the Bernstein polynomials yields then the B-form polynomial

$$p(b(\boldsymbol{x})) = \begin{cases} \displaystyle\sum_{|\kappa|=d} \alpha^t_\kappa B^d_\kappa(b(\boldsymbol{x})) & , \boldsymbol{x} \in t \\ 0 & , \boldsymbol{x} \notin t \end{cases} \tag{10}$$

of degree d on the simplex t. In order to obtain a global B-spline, a triangulation $\mathcal{T}$ of multiple adjacent simplices is constructed on the considered domain. The local B-form polynomials defined on the single simplices are joined to a smooth spline polynomial by enforcing continuity for the first r derivatives of the spline at the edges of neighbouring simplices through equality constraints

$$\mathbf{H}\boldsymbol{\alpha} = \mathbf{0}\,. \tag{11}$$

The smoothness matrix $\mathbf{H}$ contains equations establishing relationships between the basis coefficients of neighbouring simplices [De Visser, 2011].

3.3 Wavefront reconstruction with B-splines

The new approach proposed is to approximate wavefront $\phi(x, y)$ by a B-form polynomial as described in the previous section. To link the spline theory with the linearized phase retrieval problem of Section 3.1, the phase is expanded using Bernstein polynomials in (3). The wavefront is reconstructed on the aperture plane, which is divided into N equal and adjacent square regions, each of them covering one subaperture of the Hartmann sensor. The detection plane is divided in square regions aligned to the subapertures. It is assumed at this point that propagated beams from one subaperture have minimal effect on the subimage corresponding to the neighbouring subapertures.

Hence the linear optimization problem in (6) can be solved locally to estimate the phase distribution in each of the subapertures from the corresponding subimage only. The connectivity between the estimated phases is established through the equality constraints in (11). The constraint matrix $\mathbf{H}$ is global with a sparsity that depends on the matching of the derivative degree at the edges between the different simplices.

On the square subaperture regions $n = 1, ..., N$, triangulations of J_s simplices are defined. In this paper, we use a regular Type II triangulation of 4 simplices per subaperture[De Visser, 2011]. The choice of the triangulation depends on factors like sensor geometry and number of given intensity measurements. The cost function in (6) can now be formulated for each simplex $j = 1, ..., J_s$ in subaperture n with B-coefficient vector $\boldsymbol{\alpha}^n_j$, the measured intensity pixel vector $\boldsymbol{i}_{\mathrm{meas}}{}^n_j$ and the linearization constant $\boldsymbol{c_0}^n_j$ of the respective regions on the detector plane. The local Jacobian matrix $\mathbf{C_1}^n_{jj'}$ models the effect of the phase in simplex j represented by B-coefficient vector $\boldsymbol{\alpha}^n_{j'}$ on the image in the detector plane alligned to simplex j', for $j' = 1, ..., J_s$. The reconstruction of the whole wavefront is then performed by solving the following optimization problem

$$\underset{\boldsymbol{\alpha}^{\mathrm{glob}}}{\operatorname{argmin}} ||\boldsymbol{i}^{\mathrm{glob}}_{\mathrm{meas}} - (\boldsymbol{c}^{\mathrm{glob}}_{\mathbf{0}} + \mathbf{C}^{\mathrm{glob}}_{\mathbf{1}}\boldsymbol{\alpha}^{\mathrm{glob}})||^2_2 \text{ s.t. } \mathbf{H}\boldsymbol{\alpha}^{\mathrm{glob}} = \mathbf{0}\,, \tag{12}$$

$$\text{where } \mathbf{C}^{\mathrm{glob}}_{\mathbf{1}} = \begin{bmatrix} \mathbf{C_1}^1 & & \\ & \ddots & \\ & & \mathbf{C_1}^N \end{bmatrix} \text{ with } \mathbf{C_1}^n = \begin{bmatrix} \mathbf{C_1}^n_{11} & \dots & \mathbf{C_1}^n_{1J_s} \\ \vdots & \ddots & \vdots \\ \mathbf{C_1}^n_{J_s1} & \dots & \mathbf{C_1}^n_{J_sJ_s} \end{bmatrix}.$$

The global B-coefficient vector $\boldsymbol{\alpha}^{\mathrm{glob}}$, and the linearization offset $\boldsymbol{c}^{\mathrm{glob}}_{\mathbf{0}}$ respectively intensity measurement vector $\boldsymbol{i}^{\mathrm{glob}}_{\mathrm{meas}}$, are simply created by stacking their local counterparts in corresponding order. As the imaging process is not correlated between the subapertures, the global Jacobian $\mathbf{C}^{\mathrm{glob}}_{\mathbf{1}} \in \mathbb{R}^{M\times K}$ is block diagonal, where M is the total number of intensity measurements and K the total number of B-coefficients. The blocks of $\mathbf{C}^{\mathrm{glob}}_{\mathbf{1}}$ are the local Jacobians $\mathbf{C_1}^n \in \mathbb{R}^{M_s\times J_s\hat{d}}$, where $\hat{d} = \frac{(2+d)!}{2d!}$ is the number of B-coefficients to be estimated per spline. The global smoothness matrix $\mathbf{H}$ contains the equality constraints to guarantee order r continuity between the simplices.

As proposed in [De Visser and Verhaegen, 2013], we compute a least-squares estimator which eliminates the constraint equations by projection on the nullspace of the smoothness matrix $\mathbf{H}$ through the projection matrix $\mathbf{N_H} \in \mathbb{R}^{K\times k_H}$, where k_H denotes the dimension of the kernel of $\mathbf{H}$ [De Visser, 2011]. With $\mathbf{C}^{\mathbf{H}}_{\mathbf{1}} := \mathbf{C}^{\mathrm{glob}}_{\mathbf{1}}\mathbf{N_H} \in \mathbb{R}^{M\times k_H}$, the least-squares solution for the B-coefficients of the spline based wavefront reconstruction problem from intensity measurements is then

$$\boldsymbol{\alpha}^* = \mathbf{N_H}((\mathbf{C}^{\mathbf{H}}_{\mathbf{1}})^{\mathrm{T}}\mathbf{C}^{\mathbf{H}}_{\mathbf{1}})^{-1}(\mathbf{C}^{\mathbf{H}}_{\mathbf{1}})^{\mathrm{T}}(\boldsymbol{i}^{\mathrm{glob}}_{\mathrm{meas}} - \boldsymbol{c_0}^{\mathrm{glob}})\,. \tag{13}$$

The reconstruction matrix $\mathbf{R} := \mathbf{N_H}((\mathbf{C}^{\mathbf{H}}_{\mathbf{1}})^{\mathrm{T}}\mathbf{C}^{\mathbf{H}}_{\mathbf{1}})^{-1}(\mathbf{C}^{\mathbf{H}}_{\mathbf{1}})^{\mathrm{T}}$ of the estimated B-coefficients can be precomputed for the given Hartmann sensor geometry. The estimated phase values can now be obtained with (10) at any desired vector of N' locations $\boldsymbol{x} \in \mathbb{R}^{N'\times 2}$ in the cartesian plane through

$$\phi^*(\boldsymbol{x}) = \mathbf{B}(\boldsymbol{x})\boldsymbol{\alpha}^*, \tag{14}$$

where $\mathbf{B}(\boldsymbol{x})$ contains the respective Bernstein basis functions $B^d_\kappa(b(\boldsymbol{x}))$ pre-evaluated at $\boldsymbol{x}$.

4. ACCELERATION STUDY THROUGH COMPRESSIVE SAMPLING

The reconstruction of the global wavefront is computationally the most expensive part of an AO control loop. For the new generation of extremely large telescopes, the reconstruction problem (12) has to be solved for measurements of 10^4 sensor subapertures at an update frequency in the kHz range. To guarantee real-time applicability of the spline based method with intensity measurements, we propose two approaches to reduce the computational complexity. De Visser and Verhaegen [2012] have shown that the local nature of the B-spline framework allows highly distributed computation of the LS estimate. This method has been implemented for spline based wavefront reconstruction from slope measurements and can be extended to the method discussed in this paper. In addition to the distributed implementation for speeding up, we focus in this paper on a second strategy based on compressive sensing [Candès, 2006]. We present simulation results which show that the number of pixels used for estimation of the wavefrornt can be reduced dramatically without significant loss of accuracy and robustness of the reconstruction.
Motivated by the work of Ohlsson et al. [2012] and others who applied principles of the theory of compressive sensing and sampling to solve the phase retrieval problem, we only use $M' := \frac{cr}{100}M$, for $0 < cr \leq 100$, of the total number of M given intensity measurements stored in $\boldsymbol{i}^{\text{glob}}_{\text{meas}}$ to estimate the spline coefficients. This is implemented by introducing a selection matrix $\mathbf{S} \in \mathbb{R}^{M' \times M}$ in the cost function of the global reconstruction problem in (12), which yields a new cost function

$$J^{\text{CS}}_{\text{lin}} = ||\mathbf{S}(\boldsymbol{i}^{\text{glob}}_{\text{meas}} - \boldsymbol{c}^{\text{glob}}_{\mathbf{0}}) - \mathbf{S}\mathbf{C}^{\text{glob}}_{\mathbf{1}}\boldsymbol{\alpha}^{\text{glob}}||^2_2 \,. \tag{15}$$

Parameter cr denotes the undersampling of the intensity images and is further referred to as compression ratio. The LS estimate of the B-coefficient vector is then computed as

$$\boldsymbol{\alpha}^{*} = \mathbf{N}_{\mathbf{H}}\big((\mathbf{C}^{\text{CS}}_{\mathbf{1}})^{\text{T}}\mathbf{C}^{\text{CS}}_{\mathbf{1}}\big)^{-1}(\mathbf{C}^{\text{CS}}_{\mathbf{1}})^{\text{T}}\mathbf{S}(\boldsymbol{i}^{\text{glob}}_{\text{meas}} - \boldsymbol{c}^{\text{glob}}_{\mathbf{0}}) \,, \tag{16}$$

where $\mathbf{C}^{\text{CS}}_{\mathbf{1}} := \mathbf{S}\mathbf{C}^{\text{glob}}_{\mathbf{1}}\mathbf{N}_{\mathbf{H}} \in \mathbb{R}^{M' \times k_H}$ with k_H denoting the nullspace dimension of constraint matrix $\mathbf{H}$.
Choosing at each time instance, the $M'_s = crM_s$ largest intensities in each subaperture of the sensor would guarantee maximal signal to noise ratio. However, this approach is not feasible for real-time computations as it would turn the selection matrix $\mathbf{S}$ to become time variant. The consequence of this is that the reconstruction matrix $\mathbf{R}$ can no longer be precomputed, thereby increasing the real-time computational complexity (unacceptably for large scale problems such as for extremely large telescopes). Two time-invariant procedures to construct a precomputed selection matrix $\mathbf{S}$ are considered in this paper. The first is inspired by the random sampling often performed in compressive sampling [Candès, 2006]. This results in determining $\mathbf{S}$ such that at each time instance an identical (though a priori determined random) selection of M'_s pixels is made in each subaperture. The selection can differ for different subapertures. The second option is to choose the M'_s intensity measurements which are most "favoured" by the linear model in the following manner: For each subaperture n we determine a vector $\boldsymbol{k}_n \in \mathbb{R}^{M_s}$ as

$$\boldsymbol{k}_n(m) = \sum_{j=1}^{K} |\mathbf{C}_{\mathbf{1}}{}^{n}(m,j)|, \tag{17}$$

for $m = 1, ..., M_s$. The entries of this vector reflect the averaged (in terms of the $\ell 1$-norm) sensitivity of the intensity measurements to the spline coefficients corresponding to a local aperture. The selection matrix $\mathbf{S}_n \in \mathbb{R}^{M'_s \times M_s}$ is in this second option constructed such that the M'_s pixels $\boldsymbol{i}^{n}_{\text{meas}}(m)$ with the highest values for $\boldsymbol{k}_n(m)$ are selected. The global block diagonal selection matrix is given by

$$\mathbf{S} = \mathbf{diag}\,[\mathbf{S}_1, \cdots, \mathbf{S}_N] \in \mathbb{R}^{M' \times M} \,. \tag{18}$$

The motivation for the second selection option is that the "most sensitive" pixels will also be those that have the best signal to noise ratio. This heuristic argument will be further illustrated in the experimental Section 5, where a significant advantage of the Jacobian based over the randomly computed selection matrix is shown.

5. NUMERICAL SIMULATIONS

For the simulations, the same setup of a Hartmann sensor with 10 by 10 subapertures sensing at a wavelength of $\lambda = 638$nm as in [Polo et al., 2012] was considered. Each Hartmann hole has a side length of 200µm and is separated by a distance of 526.5µm from the adjacent hole. The distance of propagation between the aperture plane and the detector plane of the sensor is 10mm. Each subaperture corresponds to a square domain of 25 by 25 pixels in the detector plane. The measurement noise introduced by read out and photon noise in the sensor is modeled as a zero mean Gaussian distribution of standard deviation $\sigma_{\text{ccd}} = 4 \times 10^{-4}$, based on the specification of a commercial camera, which is added onto the normalised intensity measurements.
An astigmatism, the 4th Zernike mode in Noll's notation, is used to model the incoming wavefront with small aberrations of $\alpha_4 = 0.1\lambda$ where α_4 denotes the 4th Zernike coefficient. It was shown by Silva et al. [2013] that the spline based method for intensity measurements provides stable results for aberrations smaller than λ. The wavefront is approximated on the sensor's aperture plane with a B-form polynomial of degree $d = 2$, subject to continuity constraints of order $r = 0$. Note at this point that all results presented in this paper can also be obtained for higher order aberrations if the spline degree is increased to the radial degree of the used Zernike modes and continuity of the same order is imposed [Silva et al., 2013]. To evaluate the performance of the wavefront reconstruction the RMS values of the residual wavefront, the difference between the simulated and the estimated phase screen (both normalised to the wavelength λ), have been computed for several noise realisations to obtain an averaged result.

5.1 Selection matrix and computational gain

In this section, the advantage of the Jacobian based selection matrix $\mathbf{S}$ over its randomly computed counterpart is shown. It becomes especially significant for the compression ratios of interest $cr < 20\%$. Further, a short complexity analysis of the real-time computations which have to be performed in the presented reconstruction method shows the acceleration achieved with the compressive sampling

approach.
In Figure 2, the RMS values of the normalised residual

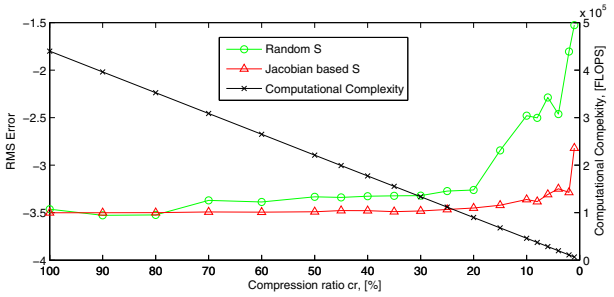

Fig. 2. RMS errors between the reconstructed and the orginal Zernike wavefront for decreasing percentage $cr\%$ of intensity measurements used. Triangles: Randomly computed selection matrix. Circles: Jacobian based selection matrix. Crosses: Real-time computational complexity depending on $cr\%$.

wavefront are plotted in logarithmic scale for wavefront estimates computed with $cr\%$ of the noisy CCD image pixels simulated for the described Hartmann setup and an astigmatic incoming wavefront. One can see, that the accuracy of the estimation performed for randomly selected pixels decreases already for less than 20% of compression ratio, whereas the Jacobian based selection matrix provides stable results up to 10% and shows a steep increase in the RMS error only at a compression ratio of 1%. Even though these results do not replace a full analysis of the Jacobian based selection, they give sufficiently strong indication to use this approach for the compressive sampling in this paper.
Next to the evolution of the RMS error, the computational complexity of the real-time computations (which have to be performed in order to obtain the values of the estimated wavefront at N' points stacked in coordinate vector $\boldsymbol{x} \in \mathbb{R}^{N'\times 2}$) is shown in Figure 2 for decreasing compression ratio cr. This real-time computations consist of applying (14) and (16), where the product $\left(\mathbf{B}(\boldsymbol{x})\mathbf{N_H}\right) \in \mathbb{R}^{N'\times k_H}$ of the spline evaluation matrix and the nullspace projector as well as the pseudo-inverse $\left(\mathbf{C_1^{CS}}\right)^+ \in \mathbb{R}^{k_H\times M'}$ of the modified Jacobian are precomputed. The selection of M' intensities with sparse matrix $\mathbf{S}$ and the subtraction of the respective linearization offsets can be scaled at M' FLOPs (Floating Point Operations). The computational complexity is then given by $\mathcal{C} = \left(N'k_H + k_H M' + M'\right)$FLOPs where the compressed total number of intensity measurements is $M' = crM_sN$ with $M_s = 625$ pixels per subaperture and $N = 100$ subapertures in the considered case. Note that for a real case scenario of an extremely large telescope N scales with $\mathcal{O}(10^4)$. The real-time computation is applied in the described way as dimension k_H of the nullspace of constraint matrix $\mathbf{H}$ is much smaller than K and M'. k_H is a function of the total number of simplices and internal edges in the triangulation as well as degree d and continuity order r of the spline model [De Visser and Verhaegen, 2013] and equals 6 for the chosen setup and model. For p evaluation points per subaperture the computational complexity is obtained with $\mathcal{C} = \left(p\,k_H N + (k_H + 1)M_s N cr\right)$FLOPs as linearly decaying function of compression ratio cr, which is plotted for $p = 4$ evaluation points per subaperture in Figure 2.

5.2 Open-loop comparison

In the following section, we present simulation results for open-loop reconstruction which show that the spline based method for intensity measurements with compressive sensing of ratio $cr = 10\%$ suffers only minor to negligible losses in peformance to variations in aberration strength and to different noise standard deviations, compared to the original method using the full CCD output. To allow further comparison to a standard wavefront reconstruction method, a modal reconstruction method using slope measurements was used for the same setup. It approximates the averaged slopes of the wavefront seen by each Hartmann subaperture computing the center of gravity of the respective intensity distributions. From these slope measurements the wavefront which is parametrized with Zernike polynomials can be estimated by solving the LS problem for optimal weighting coefficients.
Figure 3 shows the RMS values of the absolute error maps

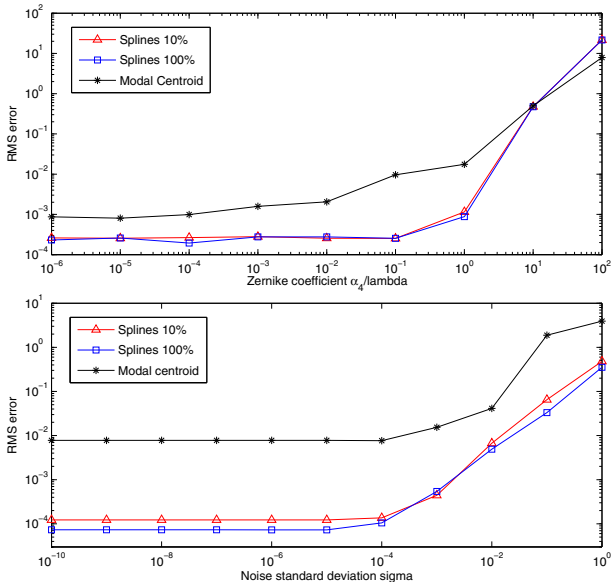

Fig. 3. RMS errors for WFR with Spline based method for 10% of the intensity measurements (Triangles), spline based method using all intensity measurements (Squares), classical modal reconstruction method for slope measurements (Stars). Top: Fixed noise standard deviation, increasing aberration strength. Bottom: Fixed aberration, increasing noise level.

between the estimated wavefront and the original incoming wavefront simulated by an astigmatism. In the first plot, a fixed noise standard deviation $\sigma_{\text{ccd}} = 4{\times}10^{-4}$ was assumed while the open-loop reconstructions were performed for increasing aberration strength simulated by augmenting the Zernike weight α_4. One can see that the spline and intensity based method gives almost the same accuracy for reconstruction from 100% or 10% of the measurements. For aberrations smaller than λ, the assumption of locally independent imaging holds and aberrations of higher polynamial orders can be retrieved from the intensity measurements. The centroid based method processes only information about the local slopes of the wavefront which yields a less accurate approximation. The RMS errors of both methods reach a threshold for very small aberrations due to the influence of the measurement noise. For aberrations larger than 10λ, the diffraction pattern corresponding to

one subaperture affects the intensity pattern of the neighbouring such that the assumption for independent imaging is not valid anymore. In this case, slope measurements give better information about the shape of the wavefront. The second plot shows the behaviour of the RMS error for the same simulations with a fixed $\alpha_4 = 0.1\lambda$ aberration where different noise levels on the intensity measurements were simulated. Again, the spline method shows the same behaviour using 10% of the intensity measurements as for reconstruction from all the pixels. Only a minor loss in accuracy was observed for the reduced version. Since the used spline polynomials of degree 2 cannot approximate higher modes in the wavefront, the performance reaches a limit due to fitting errors.

5.3 Closed-loop comparison

In the previous section, the presented results were obtained for open-loop reconstruction where neither a feedback loop nor a deformable mirror was included in the simulation. In this section, the discussed wavefront reconstruction methods were integrated in a classical AO feedback loop. It could be shown that the compressive sampling preserves the convergence properties and the sensitivity of the wavefront reconstruction error to noise. The closed-loop setup includes a simulator of the Hartmann sensor specified at the beginning of Section 5 which computes the intensity measurements and models the read out and photon noise. The wavefront values are then reconstructed using the presented methods. A delay was added in the loop to simulate the sensor's read out time as well as time consumed for the computations and communications in a real-time implementation. To compensate for the delay, a PI controller is integrated and tuned to minimize the delay's effect. For the correction, a perfect deformable mirror was assumed which can be adjusted without any fitting errors to the shape of the reconstructed wavefront.

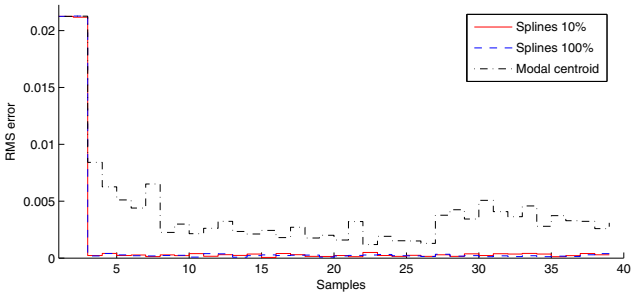

Fig. 4. RMS values of the residual wavefront for a classical closed-loop AO setup for reconstruction from intensities with the spline based method (solid: 10% of pixels; dashed: all pixels) and from slopes with the classical modal method (dot-dashed).

Figure 4 shows the results obtained for a 0.1λ astigmatism aberration with measurement noise of standard deviation 10^{-4}. The spline based method reaches the same convergence and noise sensitivity levels for the compressed number of intensity measurements as for the full number of pixels. The RMS values of reconstruction with the modal method for slope measurements emphasizes that the new intensity based spline approach converges to a lower error level and is less sensitive to noise than the classical method.

6. CONCLUSION

In this paper, we introduced a procedure to accelerate the real-time computation part of a recently presented wavefront reconstruction method for intensity measurements of a Hartmann sensor without compromising the performance of the reconstruction. The novel compressive sensing reconstruction method significantly reduces the number of intensity measurements used for wavefront reconstruction to only a small percentage of the full image information. First simulations of open- and closed-loop AO systems gave very promising results. This indicates that performance and robustness, as well as the convergence gain that was established with the new intensity based reconstruction method [Silva et al., 2013], could be preserved with a significantly reduced computational complexity. The novel compressive sensing method is highly suitable for a distributed implementation, since the selection process is independently performed for each intensity pattern in the sensor's subapertures which stands in contrast to the globally applied random sampling in many compressive sensing methods. Due to the local nature of the presented compressive sensing reconstruction method for intensity measurements, it can be integrated with our recent work of De Visser and Verhaegen [2012] who have shown that the locally defined B-spline framework allows highly distributed computation of the LS wavefront estimate.

REFERENCES

E. J. Candès. Compressive sampling. In *European Mathematical Society*, Proceedings of the International Congress of Mathematicians, 2006.

L. A. Carvalho. A simple and effective algorithm for detection of arbitrary HartmannShack patterns. *Journal of Biomedical Informatics*, 2004.

C. De Visser. *Global Nonlinear Model Identification with Multivariate Splines*. PhD thesis, Delft University of Technology, 2011.

C. De Visser and M. Verhaegen. A distributed simplex B-splines based wavefront reconstruction, 2012. URL `www.eso.org/sci/meetings/2012/RTCWorkshop6_3`.

C. De Visser and Michel Verhaegen. Wavefront reconstruction in adaptive optics systems using nonlinear multivariate splines. *Journal of the Optical Society of America A*, 30, 2013.

J. W. Goodman. *Introduction to Fourier Optics*. Roberts and Cia. Publ., 2005.

J. W. Hardy. *Adaptive Optics for Astronomical Telescopes*. Oxford University Press, Inc., 1998.

K. Hinnen, M. Verhaegen, and N. Doelman. Exploiting the spatio-temporal correlation in adaptive optics using data driven h_2-optimal control. *Journal of the Optical Society of America A*, 24, 2007.

K. Hinnen, M. Verhaegen, and N. Doelman. A data driven H2-optimal control approach for adaptive optics. *IEEE Trans. on Control Systems Technology*, 16, 2008.

H. Ohlsson, A. Yang, R. Dong, and S. Sastry. Cprl - an extension of compressive sensing to the phase retrieval problem. In *Neural Information Processing Systems*, 2012.

A. Polo, V. Kutchoukov, F. Bociort, S.F. Pereira, and H.P. Urbach. Determination of wavefront structure for a Hartmann Wavefront Sensor using a phase-retrieval method. *Optics Express*, 2012.

J. Silva, E. Brunner, M. Verhaegen, A. Polo, and C. Visser. Wavefront reconstruction using intensity measurements for real-time adaptive optics. In *ECC 2014*, 2013.

W. H. Southwell. Wavefront estimation from wavefront slope measurements. *J. Opt. Soc. Am.*, 70, 1980.